On the Relationship between Flux Emergence and CME Initiation

Yin Zhang · Mei Zhang · Hongqi Zhang

Abstract We present in this paper a statistical study aimed at understanding the possible relationship between surface magnetic field variation and CME initiation. The three samples studied comprise 189 CME-source regions, 46 active regions, and 15 newly emerging active regions. Both large-scale and small-scale variations of longitudinal magnetic fields of these regions are studied. To quantitatively study these variations, three physical quantities are calculated: the average total magnetic flux (ATF), the flux variation rate (FVR), and the normalized flux variation rate (NFVR). Our results show that 60% of the CME-source regions are found to have magnetic flux increases during 12 hours before CME eruptions and 40% are found to have magnetic flux decreases. The NFVR of CME-source regions are found to be statistically identical to those of active regions, averaged over 111 hours, and significantly smaller than those of newly emerging active regions. In addition 91% of the CME-source regions are found to have small-scale flux emergence, whereas small-scale flux emergences are also easily identified in active regions during periods with no solar surface activity. Our study suggests that the relationship between flux emergence and CME eruption is complex and the appearance of flux emergence alone is not unique for the initiation of CME eruption.

Keywords Sun: coronal mass ejection · Sun: magnetic field · Sun: activity

1. Introduction

Coronal mass ejections (CMEs) are a striking manifestation of solar activity seen in the solar corona. They were first detected in the early 1970s, and since then they have captured the attention of both the solar and the geomagnetic communities. Several review papers have been written in recent years (Forbes, 2000; Klimchuk, 2001; Low, 2001; Zhang and Low, 2005).

CMEs could be thought of as a physical mechanism by which the Sun transfers its magnetic flux and helicity, created at the base of the convective zone, into the interplanetary

Y. Zhang (✉) · M. Zhang · H. Zhang
National Astronomical Observatory, Chinese Academy of Sciences, Beijing 100012, China
e-mail: zhangyin@bao.ac.cn

medium. This large-scale eruption, which brings coronal plasma as well as associated magnetic field, would cause strong interplanetary disturbances and geomagnetic storms. These magnetic storms are the most dramatic and important component of space weather effects, which could compromise astronaut safety and lead to power outages, satellite damage, and communication failures. It is thus important for us to study the CME initiation mechanism to forecast eruptions.

Flux emergence has long been considered as an important trigger of solar activity such as flares and filament eruptions. Martin *et al.* (1982) studied the positions of 88 flares that occurred in Hale active region 16918 and concluded that at least two-thirds of the flares were intimately related to the flux emergences whereas the remaining one-third might be either indirectly related or unrelated to the flux emergences. Feynman and Martin (1995) found that in a two-month period two-thirds of the quiescent-filament-associated CMEs occurred after substantial amounts of new magnetic flux emerged in the vicinity of the filaments.

At the same time, flux cancellations, identified as magnetic reconnection on the low atmosphere, are also found to be associated with solar surface activity. The association of flares and magnetic field cancellation was first noted by Martin, Livi, and Wang (1985) and then discussed by Livi *et al.* (1989). Wang and Shi (1993) presented a scenario of two steps of magnetic reconnection in the flare process. They suggested that the observed flux cancellation presents the first step of reconnection, a slow reconnection in the lower atmosphere; the flare energy release comes directly from the second step reconnection (*i.e.*, the fast or dynamical reconnection higher in the corona). Recently, Zhang *et al.* (2001) studied a major solar event on 14 July 2000, and suggested that the flux cancellation that occurred about 10 hours before the major event is an indication of low atmosphere reconnection associated with the CME event. Wang *et al.* (2002) found a sudden disappearance of a small sunspot, associated with the 20 February 2002, M2.4 flare and suggested that the disappearing sunspot is due to rapid magnetic reconnection and subsequent submergence.

Theoretical models have also suggested that the evolution of magnetic fields at or below the photosphere, in the form of flux emergence, could result in a loss of equilibrium of the magnetic structure, which leads to a CME eruption. By 2D numerical MHD simulations, Chen and Shibata (2000) presented an emerging flux trigger mechanism for CME initiations. Their simulations show that reconnection-favored flux emergence, either within the filament channel or on the outer edge of the channel, triggers a loss of equilibrium of the flux rope and brings the formation of a current sheet below the rope. Consequent fast magnetic reconnection in the formed current sheet then leads to an eruption of the flux rope as a CME and at the same time forms a cusp-shaped arcade as is observed in X-ray flares.

Identifying changes in the photospheric longitudinal magnetic field around the times of CME eruptions has been attempted by many workers in the past. Subramanian and Dere (2001) found that active-region CMEs are often associated with small-scale flux emergences or cancellations over time scales of $6 - 7$ hours. Lara, Gopalswamy, and DeForest (2000) computed the magnetic fields of seven CME-associated active regions and one disappearing filament region and found that changes in the mean magnetic flux, ranging from ≈ 0.4 to $\approx 3.1 \times 10^{17}$ Mx per pixel (≈ 4 arcsec^2), occurred in structures whose sizes are smaller than active regions, during a period of several hours to several days. Green *et al.* (2003) studied four young active regions during their disk passage and found that the majority of CMEs and flares occurred during or after new flux emergences. Muglach and Dere (2005) studied 32 CME-source regions and found that 28 of them are associated with flux changes. These flux changes all occurred in small-scale regions and happened several hours before CME eruptions; some even continued after the CME events.

In this paper we study a large sample of 189 CME-source regions that are responsible for earth-directed halo CMEs of solar cycle 23 (1997 – 2005, inclusive). We pay particular

attention to the surface flux variations during the periods of 12 hours before CME eruptions. We study both large-scale (whose typical size is of arcminutes) and small-scale (whose typical size is of arcseconds) flux variations. We also compare our results with two other comparative samples, a sample of 46 active regions and another of 15 newly emerging active regions, to understand the uniqueness of the relationship between the surface flux variation and CME initiation. We organize our paper as follows. In Section 2 we introduce the samples we will study in this paper. In Section 3 we present the results of large-scale flux variations and in Section 4 we present the results of small-scale flux variations. A discussion and conclusion will be given in Section 5.

2. The Samples

2.1. CME-Source Regions

Many authors have studied the relationship between CME and solar surface activity. More recently, Zhou, Wang, and Cao (2003) studied the relationship between CMEs and solar surface activity and listed 197 front-side halo CMEs (1997–2001) whose associated near-surface activity could be clearly identified from the SOHO EUV Imaging Telescope (EIT) and other space-borne and ground-based observations. Gopalswamy, Yashiro, and Akiyama (2007) studied the geoeffectiveness of 378 halo CMEs (1996–2005) and give a list of them in their paper. The sample of CME-source regions we studied in this paper is extracted from these two tables. We study the surface magnetic field variation of these CME-source regions during the period of 12 hours before CME eruptions. During this process, we have corrected for the projection effect in all studied regions, details of which will be described in the following. For that purpose, we constrain ourselves to study regions within 60° of the solar disk center. This then leaves us with 189 CMEs in our sample.

2.2. Active Regions

For the purpose of space weather we need to know whether or not the surface field evolution we identified is unique to CME initiation. So we construct a sample of active regions for which we can study their long-term variations during their passage across the solar disk. These regions are selected from CME-source regions by two criteria. The first criterion is that it is an active region. The second is that its longitude at the time of the CME eruption lies between W10° and W50°, so that we can study the long-term variation of magnetic field before the eruption. This then leaves us with 46 active regions. For this sample, we study the surface magnetic field variation during the period from 96 hours before CME eruption to 15 hours after CME eruption (111 hours in total). During the period of 111 hours, most active regions show a flux increase and then a decrease. We then divide the long-term evolution of these active regions into two phases: a magnetic flux increase phase and a magnetic flux decrease phase. We then use them as the standard variation of magnetic field in active regions.

2.3. Newly Emerging Active Regions

Since we are particularly interested in understanding whether CME initiation has a close relationship with flux emergence, we construct another sample of 15 newly emerging active regions and use them as the standard for fast flux emergence. These regions are identified

from MDI movies. To get accurate correction for projection effects of MDI full-disk magnetograms and to study the emergence of the active regions as long as possible, we select regions that first appear on the east hemisphere and 30° farther from the solar limb. The developing phase of these regions lasts $50-160$ hours and the average value is 110 hours. For these active regions, we only study their developing phase and use their flux increase rate during this period as an indication of the upper limit of magnetic flux increase rate in active regions.

3. Large-Scale Flux Variations

3.1. MDI Data Reduction

As we mentioned earlier, we use full-disk longitudinal photospheric magnetograms obtained by MDI to give a quantitative investigation of longitudinal magnetic flux variations. The full-disk MDI magnetograms we use in this paper have a cadence of 96 minutes with a spatial resolution of $\approx 2''$. We carry out the following further data reductions in addition to the typical procedures carried out by the MDI team:

1. MDI magnetograms data suffer from instrumental effects. It is found that MDI underestimates magnetic flux densities in a linear way by approximately a factor of 1.54 for pixels whose flux densities are below 1200 gauss (Berger and Lites, 2003). Nindos, Zhang, and Zhang (2003) presented a nonlinear correction formula to correct the MDI flux:

$$B_{\text{corrected}} = 1.45(B + 0.23B), \quad \text{if } |B| > 1200 \text{ gauss}, \tag{1}$$

$$B_{\text{corrected}} = 1.45B, \quad \text{if } |B| < 1200 \text{ gauss}. \tag{2}$$

We follow their correction to recalibrate those MDI data used in this paper.

2. Following Chae (2001) and Chae *et al.* (2001), we align all the data by a nonlinear mapping that takes into account the solar differential rotation effect. This procedure is effective in correcting for the geometrical foreshortening originating from the spherical geometry of the Sun. Applying this procedure gives data with a new grid of $1''$ per pixel and a vertical field strength now equal to the original line-of-sight field strength times $1/\cos\psi$, where ψ is the heliocentric angle of the studied region. The interpolation of magnetograms makes identification of small-scale flux emergence or cancellation easier. We have checked that the differences of magnetic flux of the grid between $1''$ and $2''$ is less than one percent. Moreover, the size of the small-scale flux variation is much larger than $2''$, so the interpolation will not introduce fake information.

3.2. Parameter Calculation

For each studied region in each sample we calculate three parameters to quantitatively describe magnetic flux variation: the average total magnetic flux (ATF), the flux variation rate (FVR), and the normalized flux variation rate (NFVR).

1. The ATF ($\overline{\Phi}$) is defined as the total unsigned magnetic flux of the studied region, averaged over a period of time:

$$\overline{\Phi} = \frac{\sum_{i=1}^{m} \Phi_i}{m}, \tag{3}$$
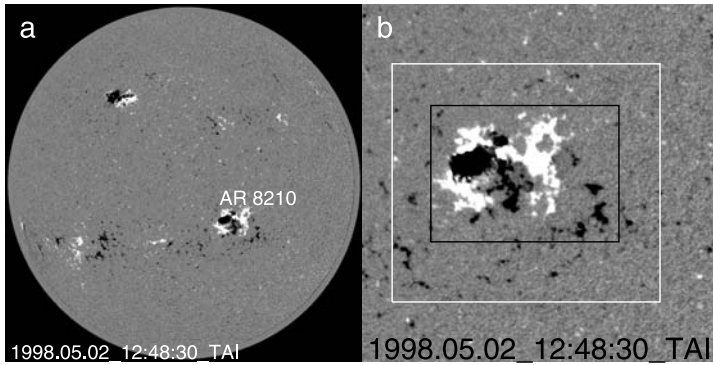
Figure 1 (a) Full-disk magnetogram obtained by MDI at 12:48 UT on 02 May 1998. (b) A CME-source region of active region 8210 with projection effect correction. Its FOV is $600'' \times 600''$. The black square indicates a FOV of $320'' \times 230''$ and the white square indicates a FOV of $450'' \times 400''$.

where m is the number of studied magnetograms of this region and $\Phi = \sum_{j=1}^{n} (|B_j|) \cdot s$. Here n is the number of pixels in each magnetogram, B_j is the magnetic flux density of the jth pixel, and s is the area in square centimeters corresponding to $(1'')^2$ on the solar surface.

To calculate the total unsigned magnetic flux, we need to remove the effect of noise. We compute the median value of the unsigned magnetic flux density ($\overline{|B_j|}$) in an area of each magnetogram outside the active region and regard it as the noise of that magnetogram, that is, B_{noise}. Then we remove the contribution of this noise from the calculation of unsigned fluxes. Therefore we have

$$|B_{j,\text{corrected}}| = 0, \quad \text{if } |B_j| < B_{\text{noise}}, \tag{4}$$

$$|B_{j,\text{corrected}}| = |B_j| - B_{\text{noise}}, \quad \text{if } |B_j| > B_{\text{noise}}. \tag{5}$$

2. The FVR ($\frac{d\Phi}{dt}$) is the variation rate of total unsigned flux over a period of time, calculated from a linear fitting of the total unsigned flux versus time. It has units of Mx h^{-1}. The sign of this parameter represents the flux variation tendency, with positive representing magnetic flux emergence and negative representing magnetic flux cancellation.

3. The NFVR ($\frac{d\Phi}{\Phi dt}$) is the ratio of the FVR ($\frac{d\Phi}{dt}$) to the ATF ($\overline{\Phi}$). It has units of h^{-1}. It has the same sign as FVR but has been normalized by the total unsigned flux of each region. It indicates a rate of variational flux to preexisting flux, which gets rid of the effect of the ATF and makes active regions of different ATF values comparable.

In calculating the ATF we need to choose a field of view (FOV). For most source regions we use a square to define the FOV. For some complicated active regions, particularly those appearing during solar maximum, a polygonal contour is used. The FOV is always the same for one source region. But it varies from a few square arcminutes to over 100 square arcmin for different source regions.

We notice that the size of the FOV we choose may influence the value of the ATF that we will obtain. We show an example of this effect in Figure 1, where a full-disk magnetogram of MDI at 12:48 UT on May 02, 1998, is displayed in Figure 1(a) and a CME-source region (AR NOAA 8210) located at the southwest of the solar disk is displayed in Figure 1(b). Here we have chosen a large FOV ($600'' \times 600''$) of this CME-source region and we displayed in Figure 1(b) the MDI magnetogram after projection correction. We then further consider two smaller FOVs. One has a size of $450'' \times 400''$, defined by the white square in Figure 1(b),

Table 1 The influence of field of view.

FOV	ATF (10^{21} Mx)	FVR (10^{21} Mx h^{-1})	NFVR (1 h^{-1})
$600'' \times 600''$	22.1	0.05	0.002
$450'' \times 400''$	21.4	0.04	0.002
$320'' \times 230''$	20.2	0.04	0.002

and the other has a size of $320'' \times 230''$, defined by the black square in Figure 1(b). We show in Table 1 the three parameters obtained for these three different FOVs. From the table we can see that the size of the FOV does have a small influence on the values of ATF and FVR obtained, but it has little influence on the NFVR. These influences are minor and should not affect our statistical result in this work.

Figure 2 shows an example of a linear combination of each sample. The three panels have the same coordinate axes: The x-axis is time and the y-axis is the unsigned magnetic flux in units of 10^{21} Mx. The ATF is the average value of marked points, the FVR is the slope of declining line, and the NFVR rate is the quotient of the former parameters.

The top panel of Figure 2 shows the ATF evolution during the 12 hours before the 14 October 1999, CME eruption. Plus symbols in this panel represent the unsigned magnetic flux calculated from MDI magnetograms and the thin solid line presents the linear fitting to these points. During these 12 hours before the CME eruption there are eight MDI full-disk magnetograms that we used and the ATF is obtained by averaging the unsigned magnetic flux of these magnetograms. For this event, the obtained ATF is 50.3×10^{21} Mx. The FVR is obtained from the slope of the fitted line and the NFVR is just this rate divided by the obtained ATF. The calculated FVR of this event is 0.45×10^{21} Mx h^{-1} and the NFVR is 0.009 h^{-1}.

In a similar way, the middle panel of Figure 2 shows the magnetic flux evolution of active region NOAA 8214. Magnetic flux of this active region reaches its maximum at about 11:12 UT on 02 May 1998 (marked by a vertical straight line in this panel). We divide the evolution of this active region into two phase: a magnetic flux increase phase, from 19:12 UT on 29 April 1998, to 11:12 UT on 02 May 1998, and a magnetic flux decrease phase, from 11:12 UT on 02 May 1998, to 12:48 UT on May 04, 1998. We then calculate the three parameters in these two phases, respectively. The solid lines in this panel show the linear fitting in these two phases, respectively. For this active region, the total averaged magnetic flux is 28.9×10^{21} Mx, the FVR is 0.14×10^{21} Mx h^{-1}, and the NFVR is 0.005 h^{-1} for the flux increase phase, and these parameters are 30.7×10^{21} Mx, -0.11×10^{21} Mx h^{-1}, and -0.004 h^{-1}, respectively, for the flux decrease phase.

Similarly, the bottom panel in Figure 2 shows the magnetic flux evolution of an active region in our newly emerging active region sample. This active region, NOAA 10119, emerges on 16 September 2002, as a dipole and then develops rapidly into a beta-gamma region on 17 September 2002. From September 16 to September 18 it produces four C-class flares and each of them is associated with a CME. The magnetic flux of this active region reaches its maximum at 01:35 UT on 22 September 2002, and we calculate its three parameters in the flux increase phase as 25.9×10^{21} Mx, 0.22×10^{21} Mx h^{-1}, and 0.009 h^{-1}, respectively.

3.3. Results

A scatter plot of the FVR and the NFVR of all three samples is shown in Figure 3. The x-axis for the FVR has units of 10^{21} Mx h^{-1} and the y-axis for the NFVR has units of 1 h^{-1}. Open and filled circles indicate CME-source regions and active regions, respectively, with

Figure 2 Total flux variation of three active regions, illustrating how the three parameters (ATF, FVR, and NFVR) are calculated. Top: Magnetic flux evolution of active region NOAA 8371 during the 12 hours (from 22:24 UT on 13 October 1999, to 09:36 UT on 14 October 1999) before the CME initiation. The solid line represents the linear fitting to the points shown. Middle: Magnetic flux evolution of active region NOAA 8214 (from 19:12 UT on 29 April 2002, to 12:48 UT on 04 May 2002). The vertical line indicates the time when magnetic flux reaches its maximum. The solid lines here represent the linear fittings to the flux points in increasing and decreasing phases, respectively. Bottom: Magnetic flux evolution of a newly emerging active region NOAA 10119 (from 23:59 UT on 15 September 2002, to 22:23 UT on 22 September 2002). The vertical line indicates the time when magnetic flux reached its maximum and the solid line represents the linear fitting to the flux points in the emerging phase of the active region.
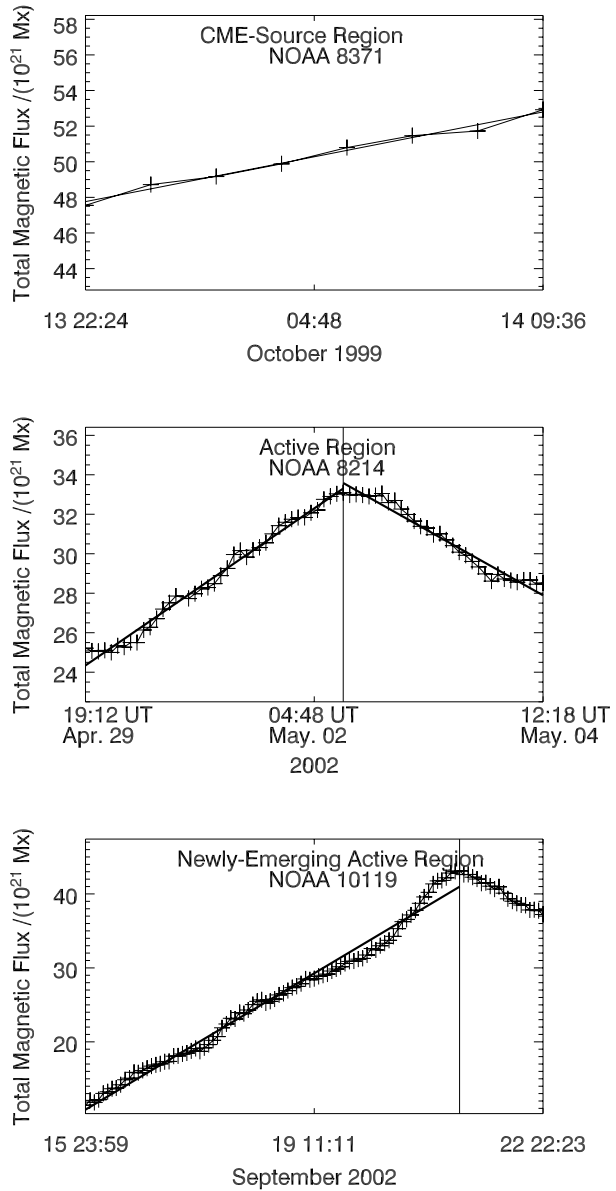
their radius in proportion to their respective ATF values. Diamonds indicate newly emerging active regions, also with their sizes in proportion to their respective ATF values. From this figure we first see that there is no significantly dominant tendency between $\frac{d\Phi}{dt} > 0$ for flux increase and $\frac{d\Phi}{dt} < 0$ for flux decrease. Out of the 189 CME-source regions studied, there are 113 (60%) regions showing a magnetic flux increase, and there are 76 (40%) showing a magnetic flux decrease. That is, both magnetic flux emergence and cancellation could exist in CME-source regions before their eruptions, although the number of CME-source

Figure 3 A scatter plot of FVR and NFVR for regions in the three studied samples. Open circles represent CME-source regions, filled circles active regions, and diamonds newly emerging active regions; their sizes are in proportion to their respective ATF values.
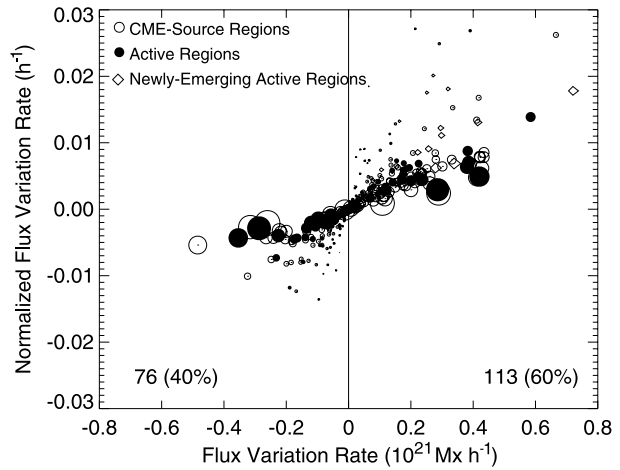
Table 2 Large-scale flux variations.

| Sample	ATF (10^{21} Mx)	FVR (10^{21} Mx h^{-1})	NFVR (1 h^{-1})	Flux variation
CME-source regions	34.4	0.13	0.005	Increase
	33.6	−0.11	−0.004	Decrease
Active regions	36.3	0.16	0.005	Increase
	39.2	−0.09	−0.003	Decrease
Newly emerging regions	25.7	0.28	0.012	Increase

regions that exhibit a flux increase is a little more than that exhibiting a flux decrease. This indicates that we will lose the trigger indicator if we look at the large-scale flux variations alone.

The figure further shows that FVR and NFVR for CME-source regions are identical to those of active regions, although values in these two samples are systematically smaller than those of the newly emerging active regions. Furthermore, the linear correlation between these two parameters (FVR and NFVR) is also obvious, especially when we sort regions into according to their ATF values. It is not surprising that FVR and NFVR are proportional one to another if ATF is constant. From the figure we still cannot find any positive correlation between ATF and CME productivity. The large scatter presented in this plot suggests that even the FVR and the NFVR give little hint as to whether or not a CME will take place.

This result is further illustrated in Table 2, where average values of the three calculated parameters are shown for all three samples. In calculating the averages, we have separated CME-source regions with positive $\frac{d\Phi}{dt}$ from those of negative $\frac{d\Phi}{dt}$ and calculated their average separately. For active regions, we average the flux increase rates and flux decrease rates separately. From this table we see again that the flux increase and decrease rates of CME-source regions are not much different from those of active regions, although both are smaller than those of newly emerging active regions.

The three panels in Figure 4, from top to bottom, show scatter plots of (1) ATF versus velocity of CMEs, (2) absolute value of FVR versus velocity of CMEs, and (3) absolute value

Figure 4 Scatter plots of velocity versus ATF (top), absolute value of FVR (middle), and NFVR (bottom). The plus symbols represent cases with positive FVR values and star symbols represent cases with negative FVR values.
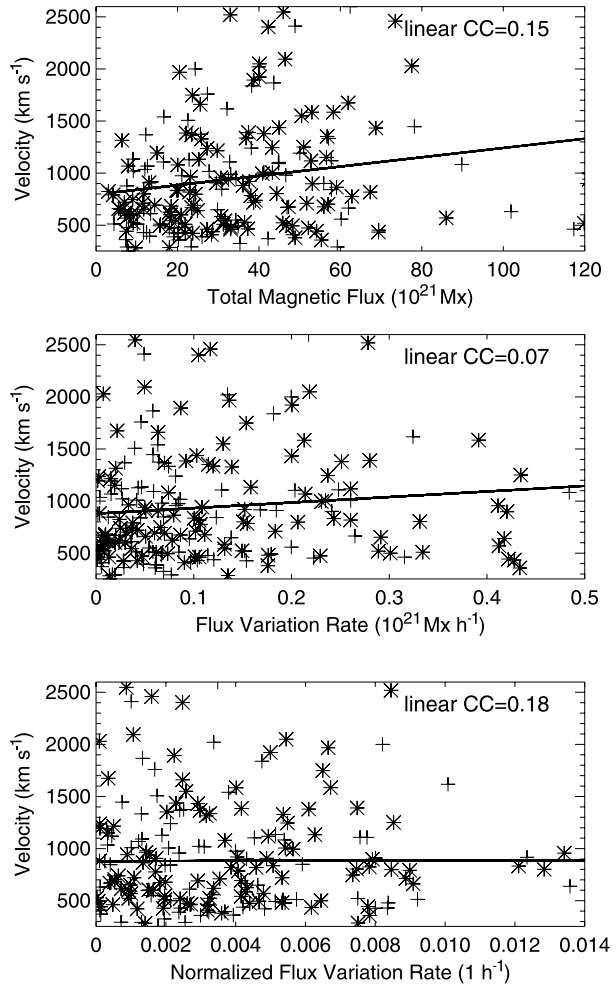
of NFVR versus velocity of CMEs, where plus symbols represent cases of ATF increase and star symbols represent cases of ATF decrease. The solid lines show the least-squares linear fittings to the data points, and the correlation coefficients of the data points are also presented in each panel. Apparently, there is no positive correlation between the three parameters and the velocity of CMEs, further demonstrating the complexity of the relationship between flux emergence or cancellation and CME onset.

Out of the 189 CME-source regions, 22 active regions are found to produce more than one CMEs. Namely, there are 83 CMEs that originated from the 22 active regions. We then calculated the time interval and the flux variation between two CMEs that originate in same source region. We find that, in the flux increase phase, the average value of the time interval is 37.2 hours and the average value of the relative flux variation of the total flux is 14%; meanwhile, in the flux decrease phase, the CME occurred after an interval of 41.6 hours and the relative flux variation of the total flux is 10% on average.

4. Small-Scale Flux Variation of CME-Source Regions

4.1. Small-Scale Flux Emergence and Cancellation Identification

As we do not find in the previous section a unique relationship between the large-scale (on a scale of several arcminutes) flux variation and CME initiation that would be useful for space weather purposes, we go further in this section to search for small-scale (on a scale of several arcsecs) flux variations that might be associated with CME initiation. We manually screened the magnetic field evolutions of the 189 CME-source regions during the period of 12 hours before their eruptions and searched for small-scale flux emergences and cancellations in these regions. In this study, we only consider the obvious changes of flux, such as newly flux emergence, complete cancellation, and changes that can be easily identified by eye from contrast-enhanced MDI movies.

Figures 5(a) to (c) show an example where both small-scale flux emergence and cancellation have been identified in a CME-source region during the 12 hours before CME eruption. This is the active region NOAA 8371 where the 14 October 1999, CME originates. The white squares in the four panels of this figure indicate where a positive-polarity flux is found to emerge into a negative-polarity flux. The black squares in each panel outline where flux cancellation has been identified. An EIT 284 Å image of the flare is shown in Figure 5(d) at 09:00 UT. The corresponding MDI longitudinal magnetogram is overlaid on the EIT image in this panel to show the magnetic field clearly. From this panel, it is interesting to find that both flux emergence and flux cancellation take place in the flaring region of the CME-associated flare. A region like this one, with obvious flux emergence and cancellation, is typical in our CME-source regions.
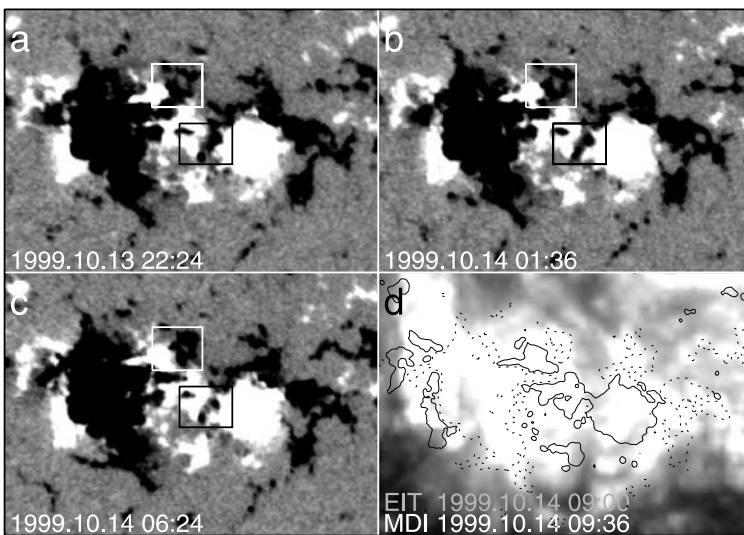
Figure 5 (a) – (c) Longitudinal magnetic field evolution before the eruption of the 14 October 1999, CME. The white squares in each panel outline the position where a small-scale flux emergence is identified. The black squares in each panel outline the position where a small-scale flux cancellation is identified. The field of view is $320'' \times 226''$. (d) EIT 284 Å image at 09:00 UT, overlaid with corresponding MDI longitudinal magnetogram. Contours of solid and dashed lines represent positive and negative magnetic fields, respectively.

4.2. Results

After we screened each CME-source region and identified small-scale flux emergence and cancellation in these regions, we then sorted these CME-source regions into four categories: I. regions where only small-scale flux emergence can be identified, II. regions where only small-scale flux cancellation can be identified, III. regions where both flux emergence and cancellation have been identified, and IV. regions where neither flux emergence nor cancellation are identified. We find that, out of the 189 regions studied, only 5% are identified with only small-scale flux emergence in their source regions. Also only 5% are identified with only small-scale flux cancellation in their source regions, and 4% are identified as having neither small-scale emergence nor small-scale flux cancellation. The vast majority, that is, 86% of CME-source regions, show both small-scale flux emergence and small-scale flux cancellation. That is, in our sample, 91% of CME-source regions show small-scale flux emergence during the 12 hours before the CME eruption, and about the same amount of CME-source regions show small-scale flux cancellation during the 12 hours before CME initiation.

The high percentage of small-scale flux emergence identified seems to suggest that there is a close relationship between small-scale flux emergence and CME initiation, a point that has been suggested by several previous observational and theoretical studies (Subramanian and Dere, 2001; Green *et al.*, 2003; Chen and Shibata, 2000). However, if we want to use this relationship for space weather purposes, we need to identify whether this relationship is unique to CME eruptions. For this purpose, we also screen the 46 active regions and search for small-scale flux emergence in the same way as we did for CME-source regions. We find that small-scale flux emergence is an ubiquitous phenomena during active region evolution. We can only identify eight time slices in five active regions where no small-scale flux emergence was identified during a period of 12 hours or longer. For other active regions, or other periods of evolution for those five active regions, we can always identify one or more instances of small-scale flux emergence in the studied active region. This seems to say that small-scale flux emergence is taking place frequently over the whole period of the active region, whether or not a CME takes place.

We then go further to calculate the small-scale flux increase rate and try to see whether this rate will make the CME-associated small-scale flux emergence stand out from those in active regions. We select 34 CME-associated small-scale flux emergence events that we can identify from the very beginning of their emergence. We calculate their FVR and NFVR in the same way as we calculate large-scale variations in the previous section, except that now we calculate these numbers in a smaller region where the small-scale emergence takes place. The time periods for calculating these numbers are different from one event to another as they are emerging at different times before the CME eruptions. The average time of the calculated period is 9.7 hours. As a comparison, we also select 27 non-CME-associated small-scale flux emergence events from the sample of active regions via the same criteria. Namely, we select regions that we can identify from the very beginning of their emergence when there is no major surface activity (CMEs or X-class flares recorded by GOES) occurring in the active region, during the period of 12 hours after the flux emergence. We calculate the FVR and NFVR in these 27 small-scale regions too, from the time of their emergence to 9.6 hours (six magnetograms of a cadence of 96 minutes) after their emergence. These make these two small samples comparable, the only difference being that one is CME-associated and the other is non-CME-associated. For these events, a polygonal contour defined by eye is fitted around the small-scale emergence region. To minimize the contribution of the background field not related to the emergence, we only calculate the emerging flux whose polarity is opposite to that of the vicinity. Obviously, their FOV would vary with the emergence

Figure 6 A scatter plot of FVR and NFVR for CME-associated small-scale flux emergence (open circles) and non-CME-associated small-scale flux emergence (filled circles).
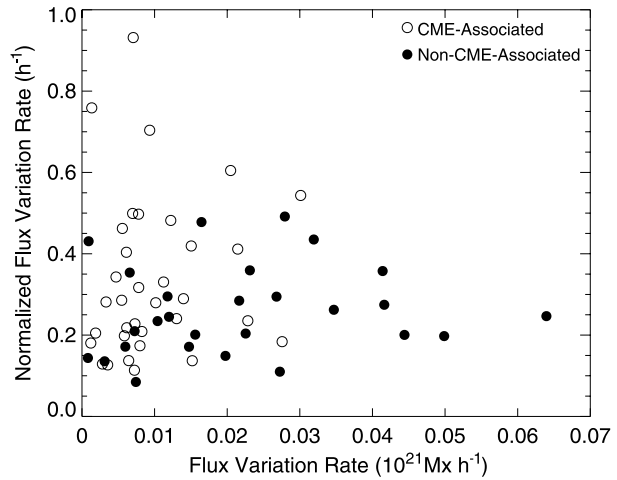
Table 3 FVR of small-scale flux emergence.

Sample	ATF (10^{21} Mx)	FVR (10^{21} Mx h^{-1})	NFVR (1 h^{-1})
CME-associated	0.036	0.010	0.340
Non-CME-associated	0.093	0.021	0.260

of the flux. A scatter plot of the FVR and the NFVR of these two small samples is shown in Figure 6. Similar to Figure 3, the open circles indicate CME-associated small-scale flux emergence and the filled circles represent non-CME-associated small-scale flux emergence. The plot shows a tendency of CME-associated regions toward higher values of NFVR and of non-CME-associated regions toward higher values of FVR. The reason for this difference is as follows: When we identify small-scale flux emergence in CME-source regions, we pay particular attention to the flaring region of the CME-associated flares. Any persistent emergence is detected, even an emergence as small as tens of arcseconds. But when we identify small-scale flux emergence in active regions, emerging flux with large size is easy to identify. This is more or less subjective, but it is difficulty to avoid. Furthermore, when we remove these two parts we can see that, again, FVR and NFVR for CME-associated and non-CME-associated regions are identical to each other. So we still do not find a unique relationship between small-scale flux emergence and CME initiation even for the FVR and NFVR.

As in Table 2, our result is further illustrated in Table 3 for small-scale flux emergence. For the 34 CME-associated small-scale flux emergence cases, ATF, FVR, and NFVR are 0.036×10^{21} Mx, 0.010×10^{21} Mx h^{-1}, and 0.340 h^{-1}, respectively. For the 27 non-CME-associated small-scale flux emergence cases, ATF, FVR, and NFVR are 0.093×10^{21} Mx, 0.021×10^{21} Mx h^{-1}, and 0.260 h^{-1}, respectively. We see again that the NFVR values are identical for the two small samples.

5. Conclusion and Discussion

We studied a sample of 189 CME-source regions in this paper. We studied both large-scale and small-scale variations of longitudinal magnetic fields, with the goal of understanding

whether there is a unique relationship between surface magnetic field variation and CME initiation. We calculated three parameters – ATF, FVR, and NFVR – to quantitatively describe the magnetic flux variations.

We find that, out of the 189 CME-source regions we studied, 60% have magnetic flux increases during the 12 hours before CME eruptions and 40% have magnetic flux decreases. The average values of FVR and NFVR of these CME-source regions are found to be identical to those of active regions. This seems to suggest that, although both flux emergence and flux cancellation could happen before CME eruptions, their appearances may just be a typical process in active region evolutions, rather than an indicator of CME initiation. Consequently, there is no positive correlation between the velocity of CMEs and the three parameters.

We have also studied the small-scale flux emergence and cancellation in CME-source regions. We find that out of the 189 CME-source regions, 91% have small-scale flux emergence within the region during the 12 hours before CME eruption, whereas the same amount (91%) of source regions have small-scale flux cancellations as well. But at the same time, we find small-scale flux emergence can also be easily identified in active regions during periods with no solar surface activity. A quantitative investigation of 34 CME-associated small-scale flux emergence cases and 27 non-CME-associated small-scale flux emergence cases shows that the NFVR values of CME-associated small-scale emergence are identical to those of non-CME-associated small-scale emergence cases.

Our study suggests that the relationship between flux emergence and CME eruption is complex and that the appearance of flux emergence alone is not unique for CME initiation. The circumstances leading to CME eruption may be sensitive not only to the appearance of newly emerging flux but also to several other factors such as the strength, distance, area of the emerging flux, and helicity of the source region as many previous researchers have proposed (Lin, Forbes, and Isenberg, 2001; Wang, Zhou, and Zhang, 2004; Zhang, Flyer, and Low, 2006). Further studies are necessary to establish a unique relationship between flux emergence and CME eruption for space weather purposes.

References

Berger, T.E., Lites, B.W.: 2003, *Solar Phys.* **213**, 213.
Chae, J.: 2001, *Astrophys. J.* **560**, L95.
Chae, J., Wang, H.M., Qiu, J., Goode, P.R., Strous, L., Yun, H.S.: 2001, *Astrophys. J.* **560**, 476.
Chen, P.F., Shibata, K.: 2000, *Astrophys. J.* **545**, 524.
Feynman, J., Martin, S.F.: 1995, *J. Geophys. Res.* **100**, 3355.
Forbes, T.G.: 2000, *J. Geophys. Res.* **105**, 23153.
Gopalswamy, N., Yashiro, S., Akiyama, S.: 2007, *J. Geophys. Res.* **112**, A06112.
Green, L.M., Démoulin, P., Mandrini, C.H., Van Driel-Gesztelyi, L.: 2003, *Solar Phys.* **215**, 307.

Klimchuk, J.A.: 2001, In: Song, P., Singer, H., Siscoe, G. (eds.) *Proc. of the Chapman Conference on Space Weather, Geophysical Monograph* **125**, American Geophysical Union, Washington, 143.

Lara, A., Gopalswamy, N., DeForest, C.: 2000, *Geophys. Res. Lett.* **27**, 1435.

Lin, J., Forbes, T.G., Isenberg, P.A.: 2001, *J. Geophys. Res.* **106**, 25053.

Livi, S.H.B., Martin, S.F., Wang, H.M., Ai, G.X.: 1989, *Solar Phys.* **121**, 197.

Low, B.C.: 2001, *J. Geophys. Res.* **106**, 25141.

Martin, S.F., Dezso, L., Antolova, A., Kucera, A., Harvey, K.L.: 1982, *Adv. Space Res.* **2**, 39.

Martin, S.F., Livi, S.H.B., Wang, J.: 1985, *Aust. J. Phys.* **38**, 929.

Muglach, K., Dere, K., 2005, In: Dere, K., Wang, J., Yan, Y. (eds.) *Coronal and Stellar Mass Ejections, IAU Symp.* **226**, 179.

Nindos, A., Zhang, J., Zhang, H.Q.: 2003, *Astrophys. J.* **594**, 1033.

Subramanian, P., Dere, K.P.: 2001, *Astrophys. J.* **561**, 372.

Wang, J.X., Shi, Z.X.: 1993, *Solar Phys.* **143**, 119.

Wang, J.X., Zhou, G.P., Zhang, J.: 2004, *Astrophys. J.* **615**, 1021.

Wang, H.M., Spirock, T., Qiu, J., Ji, H.S., Yurchyshyn, V., Moon, Y.J., *et al.*: 2002, *Astrophys. J.* **576**, 497.

Zhang, M., Low, B.C.: 2005, *Annu. Rev. Astron. Astrophys.* **43**, 103.

Zhang, M., Flyer, N., Low, B.C.: 2006, *Astrophys. J.* **644**, 575.

Zhang, J., Wang, J.X., Deng, Y.Y., Wu, D.J.: 2001, *Astrophys. J.* **548**, L99.

Zhou, G.P., Wang, J.X., Cao, Z.L.: 2003, *Astron. Astrophys.* **397**, 1057.